Arctic decadal variability in a warming world

van der Linden, Eveline C.; Bintanja, Richard; Hazeleger, Wilco

IMPORTANT NOTE: You are advised to consult the publisher's version (publisher's PDF) if you wish to cite from it. Please check the document version below.

Document Version
Publisher's PDF, also known as Version of record

Link to publication in University of Groningen/UMCG research database

JGR

Key Points:
- Dominant Arctic decadal variability shifts toward the central Arctic and Siberian regions as the climate warms
- Links between dominant atmospheric modes and Arctic climate characteristics vary strongly with climate warming
- The Aleutian Low plays a more prominent role in wintertime Arctic temperature variability in warmer climates

Correspondence to:
E. C. van der Linden,
linden@knmi.nl

Arctic decadal variability in a warming world

Eveline C. van der Linden[1] , **Richard Bintanja[1,2]**, and **Wilco Hazeleger[3,4]**

[1]Royal Netherlands Meteorological Institute (KNMI), De Bilt, Netherlands, [2]Energy and Sustainability Research Institute Groningen, University of Groningen, Groningen, Netherlands, [3]Meteorology and Air Quality Group, Wageningen University and Research, Wageningen, Netherlands, [4]Netherlands eScience Center, Amsterdam, Netherlands

Abstract Natural decadal variability of surface air temperature might obscure Arctic temperature trends induced by anthropogenic forcing. It is therefore imperative to know how Arctic decadal variability (ADV) will change as the climate warms. In this study, we evaluate ADV characteristics in three equilibrium climates with present-day, double, and quadrupled atmospheric CO_2 forcing. The dominant region of variability, which is located over the Barents and Greenland Sea at present, shifts to the central Arctic and Siberian regions as the climate warms. The maximum variability in sea ice cover and surface air temperature occurs in the CO_2 doubling climate when sea ice becomes more vulnerable to melt over vast stretches of the Arctic. Furthermore, the links between dominant atmospheric circulation modes and Arctic surface climate characteristics vary strongly with climate change. For instance, a positive Arctic Oscillation index is associated with a colder Arctic in warmer climates, instead of a warmer Arctic at present. Such changing relationships are partly related to the retreat of sea ice because altered wind patterns influence the sea ice distribution and hence the associated local surface fluxes. The atmospheric pressure distributions governing ADV and the associated large-scale dynamics also change with climate warming. The changing character of the ADV shows that it is vital to consider (changes in) ADV when addressing Arctic warming in climate model projections.

1. Introduction

The Arctic is currently warming much faster than other parts of the world, and sea ice is rapidly diminishing [*Comiso and Hall*, 2014]. Superimposed on this warming trend is a strong decadal variability, which can reinforce or oppose the trend, depending on its phase [*Kay et al.*, 2011; *Swart et al.*, 2015]. This renders interpreting Arctic changes in terms of anthropogenically caused forcing quite uncertain. The characteristics of this Arctic decadal variability (ADV) have been investigated using observations [*Polyakov et al.*, 2003] and climate models [e.g., *Day et al.*, 2012; *Van der Linden et al.*, 2016]. There are strong indications that the ADV (expressed mainly in sea ice variability) exhibits links with other long-term modes of variability, such as the North Atlantic Oscillation (NAO) [*Holland*, 2003], Atlantic Multidecadal Oscillation (AMO) [*Li et al.*, 2013], and Pacific Decadal Oscillation (PDO) [*Day et al.*, 2012] — with a geographical imprint that seems to vary strongly between models — and with low-frequency variations in Arctic cyclone activity [*Zhang et al.*, 2004]. There is also a well-established connection with ocean-induced variability related to the Atlantic Meridional Overturning Circulation (AMOC) and related heat transports [*Zhang and Wang*, 2013], specifically in certain regions of the Arctic (the Barents Sea) [*Goosse and Holland*, 2005; *Van der Linden et al.*, 2016].

Notwithstanding its causes and governing mechanisms, the ADV not only potentially obscures trends in Arctic climate, the ADV itself might also change with climate state. As with any mode of variability, the mechanisms controlling the characteristics of the ADV are firmly rooted in the "ambient" climate state, and if this state and the associated mechanisms change (e.g., due to forced climate warming), the characteristics of the ADV will very likely change as well, possibly in conjunction with simultaneous fluctuations in the other modes of variability such as the Arctic Oscillation (AO) [*Overland and Wang*, 2005]. For instance, *Kay et al.* [2011] find that the variations in the magnitude of the Arctic sea ice trend over 2–10 years increases toward the end of the 21st century in an ensemble of forced scenario simulations, suggesting that the amplitude of the ADV will enhance with climate warming. Climate model simulations of warm paleoworlds demonstrate that ADV may be governed by high-latitude upper ocean static stability, leading to increases in both the frequency and the magnitude of ADV in warmer climates [*Poulsen and Zhou*, 2013]. To date, very little is known about the characteristics and possible causes of changing ADV toward warming climates.

In a transient climate, it is difficult to separate trends from internal climate variability. Transient climate changes also make it hard to assess ADV and its relationships to other modes, since the baseline climatologies are shifting. This uncertainty impacts the timing of the Arctic Ocean to become ice free for the first time; for instance, a strong negative trend combined with a large ADV may result in an ice-free state occurring much earlier than expected from forced trends alone [*Swart et al.*, 2015]. Furthermore, slowly changing feedbacks related to altered variability in sea ice and snow potentially modify tropospheric wave activity and the jet stream [*Cohen et al.*, 2014]. To obtain insight into the details of the ADV, and in particular, the changes therein, a fruitful approach is to eliminate the complicating effects of a slowly varying background climate. In this study, we do so by specifically focusing on equilibrium climate states with little to no residual trend. We therefore use 550 year integrations with the state-of-the-art climate model EC-Earth in 1×CO$_2$, 2×CO$_2$, and 4×CO$_2$ forcing simulations, for which we evaluate the characteristics of the ADV using the final 400 years of the simulations during which the respective climate states are in (quasi-)equilibrium. We will focus on the large-scale climate mechanisms that are involved in atmosphere-ice-ocean interactions. By using a single climate model, we can concentrate on process understanding, without having to deal with uncertainties related to structural differences in the model design (as in multimodel studies). Section 2 contains details of the model, the model simulations, and the analyses methodology. In section 3 we describe the characteristics of the ADV for the "warm" climates relative to the present-day climate. Changes in the atmospheric variability patterns are described in section 4. Links between ADV and various modes of climate variability as well as the responsible mechanisms are explored in section 5. Conclusions and possible implications of our findings are discussed in section 6.

2. Model, Simulations, and Methods

2.1. Model Description

The experiments in this study are performed with EC-Earth [*Hazeleger et al.*, 2012]. Here we use version 2.3, which has also contributed to the Coupled Model Intercomparison Project phase 5 (CMIP5) [*Taylor et al.*, 2012]. EC-Earth is a fully coupled atmosphere-ocean global climate model. The atmospheric component is the Integrated Forecast System (IFS) of the European Center for Medium-Range Weather Forecasts (ECMWF). It runs at T159 spectral resolution with 62 vertical levels. The ocean component is the Nucleus for European Modelling of the Ocean (NEMO) model [*Madec*, 2008], developed by the Institute Pierre Simon Laplace. NEMO uses a horizontal grid configuration which has a resolution of about 1° and 42 vertical levels. NEMO incorporates the Louvain la Neuve sea ice model version 2 (LIM2) [*Fichefet and Morales Maqueda*, 1997; *Bouillon et al.*, 2009], which is a dynamic-thermodynamic sea ice model. The atmosphere and ocean/sea ice model are coupled through the OASIS (Ocean, Atmosphere, Sea Ice, Soil) coupler [*Valcke et al.*, 2003].

Future projections of climate change and ocean heat transports in EC-Earth, focused specifically on the Arctic region, are analyzed in detail in *Koenigk et al.* [2013] and *Koenigk and Brodeau* [2014]. These studies show that the Arctic climate in EC-Earth is overall reasonably well simulated.

2.2. Simulations

We study three simulations performed with EC-Earth forced with different carbon dioxide (CO$_2$) concentrations (Table 1). The first integration is the control climate (CTRL) which contains greenhouse gas concentrations, aerosol forcing, and a land use scheme of the year 2000 (present day). The initial state for CTRL is obtained from a spin-up of about 1000 years with preindustrial (1850) forcing and a subsequent integration over 44 years with present-day forcing. Thereafter the integration is continued over 550 years with constant present-day forcing, which in this study we refer to as the CTRL simulation. The other two integrations start from the initial state of CTRL. Their CO$_2$ concentrations are instantaneously set at 2 (2×CO$_2$) and 4 (4×CO$_2$) times the present-day value and kept constant at that level for 550 years. After 150 years the upper ocean is close to equilibrium. We use the final 400 years in our analysis.

2.3. Methods

The data employed in this study include monthly mean Northern Hemisphere (20–90°N) sea level pressure (SLP), Arctic (70–90°N) surface air temperature (SAT), and Northern Hemisphere sea ice area (SIA) and concentration. The variables that will be shown and discussed are detrended prior to analysis to remove the remaining drift, which had almost no impact in these close-to-equilibrium climate states. To focus on the decadal time scales, all time series are smoothed with an 11 year running Welch window, which consists of a single parabolic section.

Table 1. Simulation Name, CO_2 Concentration (ppmv), the Global Equilibrium 2 m Air Temperature (T_{global}), the Arctic (70–90°N) Equilibrium 2 m Air Temperature in Winter (T_{DJF}) and Summer (T_{JJA}) in °C, and the SIA maximum (SIA_{max}) and minimum (SIA_{min}) in 10^{12} m^2

Simulation	CO_2	T_{global}	T_{DJF}[b]	T_{JJA}[c]	SIA_{max}	SIA_{min}
CTRL	368.9	14.3	−24.4	0.6	15.8	5.2
$2\times CO_2$	737.7	17.2	−9.5	4.1	10.8	0.15
$4\times CO_2$	1475.5	20.8	−1.0	9.3	0.63	0.13
ERA-20C[a]	–	13.6	−26.2	0.4	13.7	8.8

[a]Reanalysis data of ERA-20C averaged over the period 1990–2010 are included for comparison. Note, however, that the conditions of CTRL with fixed CO_2 concentration are different from the ones observed over the recent past in ERA-20C.
[b]DJF: December–February;
[c]JJA: June–August.

To examine the spatial structure of SLP and SAT variability, we use empirical orthogonal function (EOF) analysis, which (in our application) seeks spatial-temporal structures that explain most of the variability. To further assess and confirm the relationships between Northern Hemisphere SLP and Arctic SAT, we use the method of singular value decomposition (SVD) on the cross-covariance matrix between SAT and SLP. In this way, we will identify the coupled spatial patterns that explain most of the covariance between the two variables.

Throughout the paper, statistical significance was tested by bootstrapping the data 10,000 times after taking the seasonal or annual average of the monthly data. Before applying the statistical tests, the data from the original grid were averaged onto a coarser 2° by 2° grid to reduce the size of the data sets and the associated computational load. Each bootstrapped sample is smoothed so that the resampled distribution includes the effect of decadal smoothing. The resampled distributions are used to compute the statistical significance of the results.

Note that the climate change simulations analyzed here do not account for possible changes in land ice extent or elevations (Greenland and Antarctica), or for changes in vegetation, in land use, or aerosols.

3. Temperature and Sea Ice

3.1. Mean State of Temperature and Sea Ice

Sea ice plays a key role in the Arctic climate system and modulates the surface air temperature through various feedback processes. Table 1 summarizes the mean characteristics of sea ice area (SIA) and surface air temperature (SAT) for the three simulated climate states and includes reanalysis data of ERA-20C [*Poli et al.*, 2016] for comparison. ERA-20C is ECMWF's first atmospheric reanalysis of the twentieth century, spanning 1900–2010. EC-Earth overestimates the seasonal cycle in sea ice area, with too high values in March and too low values in September. The model captures summer (JJA) Arctic surface air temperatures quite well but is warmer than ERA-20C during winter (DJF). In the present-day Arctic climate, simulated SIA and SAT are closely connected. In winter, when the temperature is on average about −24°C, SIA extends to 15.8 $\times 10^6$ km^2, whereas in summer SIA shrinks to approximately one third of this area. It is also clear that in warmer climate states, the total Arctic SIA declines. Whereas in CTRL sea ice remains during the summer minimum, it is only seasonal in $2\times CO_2$, and almost completely absent throughout the year in $4\times CO_2$, with the global mean temperature increasing by 2.9°C and 6.5°C, respectively. By comparison, using an ensemble of CMIP5 global climate models with RCP8.5 forcing, *Hezel et al.* [2014] found that September sea ice disappears at a mean global temperature increase of 2.4°C and March sea ice at a mean temperature increase of 8.2°C. Although the mean winter and summer sea ice extent diminish when CO_2 concentrations increase, it is important to analyze their decadal variability to separate forced trends, caused by CO_2 rise, from the variations due to natural fluctuations. In the following, we will investigate the variability of the SAT and sea ice in warmer climate states and evaluate how these compare to the current state.

3.2. Variability of Temperature and Sea Ice

Figures 1 and 2 show time series of 2 m Arctic air temperature anomalies and Arctic sea ice area anomalies for the three different climate states in winter and summer, respectively. The anomalies are computed by removing the mean monthly climatology from the detrended monthly mean time series and decadally smoothed.
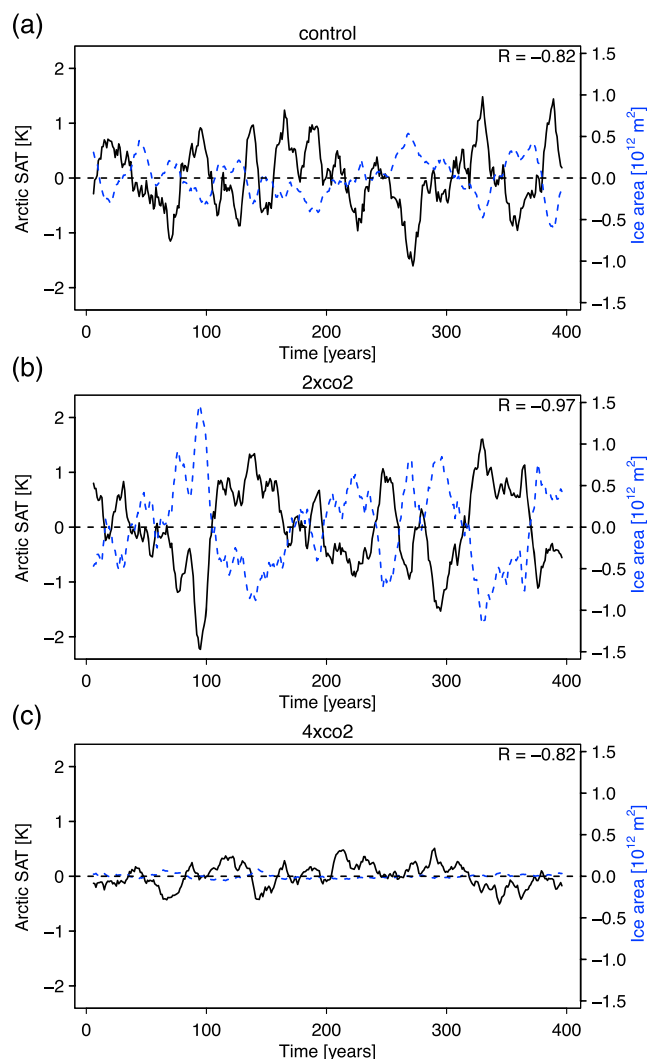
Figure 1. Time series of winter (DJF) Arctic (averaged over 70–90°N) temperature anomalies (black line) and Arctic sea ice area anomalies (blue dashed line) for (a) CTRL, (b) 2×CO$_2$, and (c) 4×CO$_2$. Time series are smoothed with an 11 year running Welch window. The correlation coefficient between Arctic SAT and SIA is indicated.

Standard deviations of these time series are listed in Table 2. Previous studies have shown that this type of decadal variability has the potential to obscure forced trends [*Swart et al.*, 2015].

In the Arctic, the presence or absence of sea ice plays a major role in surface air temperature variability. Over sea ice, summer variability is relatively small because the surface temperature is constrained by the freezing point temperature. In winter, temperature variability is larger over sea ice than over the ocean since the large thermal inertia of the ocean damps the changes. In the 4×CO$_2$ climate, the decadal variability (henceforth referred to as "variability") of temperature and SIA is similar in winter and summer, corresponding to the relatively small differences in mean sea ice area between both seasons. In the CTRL and 2×CO$_2$ climate, however, the links between sea ice and temperature variability are less straightforward. In both CTRL and 2×CO$_2$ the summer temperature variability is much smaller than in winter even though summer sea ice is almost completely absent in the 2×CO$_2$ climate (Table 1). Furthermore, while the SIA variability is much larger in winter in 2×CO$_2$ as compared to present day, and corresponding to the large winter temperature variability, the standard deviation of SIA in CTRL is the same for winter and summer. It seems as if besides the presence of sea ice, SAT variability is additionally constrained by other factors.

In order to understand the reasons behind the dependence of the temperature and sea ice variability on the mean climate state, one has to analyze the associated patterns. To examine the spatial structure of 2 m air
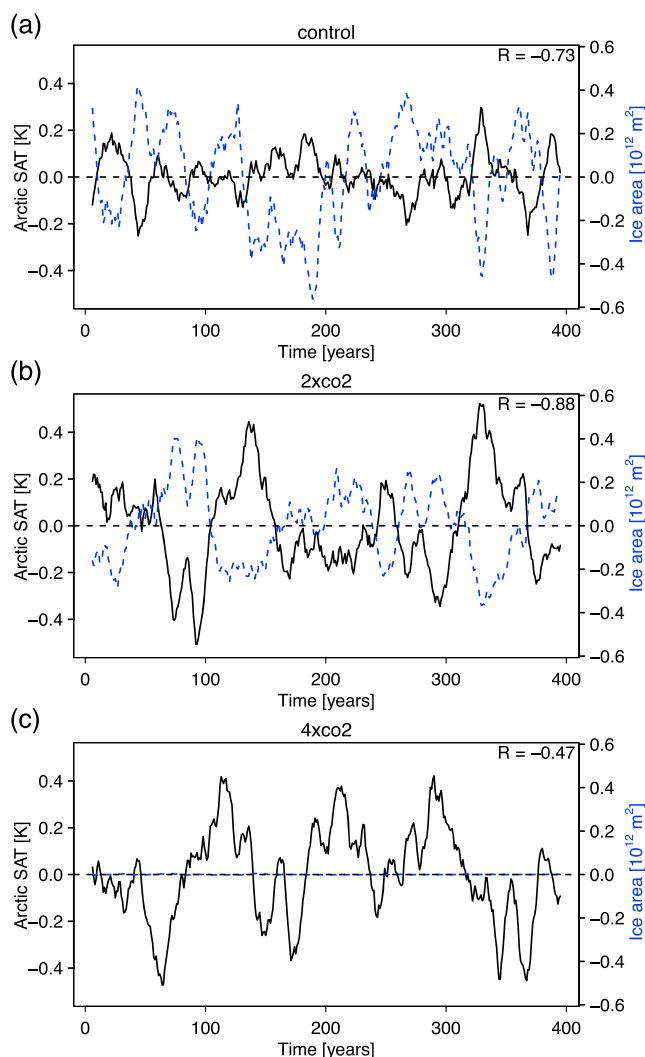
Figure 2. Time series of summer (JJA) Arctic (averaged over 70–90° N) temperature anomalies (black line) and Arctic sea ice area anomalies (blue dashed line) for (a) CTRL, (b) 2×CO_2, and (c) 4×CO_2. Time series are smoothed with an 11 year running Welch window. The correlation coefficient between Arctic SAT and SIA is indicated.

temperature variability, we use the method of empirical orthogonal function (EOF) analysis. In these analyses, EOFs are stationary fields by construction, while the principal component attached to each EOF represents the sign and amplitude of the EOF as a function of time. Each leading EOF of surface air temperature over the Arctic region (70–90°N), labeled E1(SAT), is visualized in Figure 3, by the regression of winter and summer SAT on the corresponding normalized principal component, termed e1(SAT) (Figure 4). This regression map has the shape of the EOF, but the amplitude corresponds to the amplitude of SAT in physical units with which this structure is associated. The leading EOF accounts for 37–73% of the explained variance, depending on climate state and season as indicated in Figure 3. The dominant region of variability, which in the current climate is located over the Barents Sea and the Greenland Sea, shifts more to the central Arctic and Siberia as the climate warms. Since the Arctic exhibits an outspoken seasonality in the mean climate and since also the variability depends strongly on the season, we analyze the variability in winter and summer separately.

3.2.1. Winter Variability

In winter, decadal variability of 2 m air temperature and SIA increases in 2×CO_2 as the ice cover shrinks compared to present-day conditions (Figure 1b). In even warmer climates (4×CO_2), however, when winter ice extent decreases further, the variance of both temperature and SIA drops to lower values than in CTRL (Figure 1c). Winter temperature and sea ice variability are thus nonlinearly related to the mean climate state. The correlations between Arctic winter temperature and SIA are high, ranging from −0.82 ($p < 0.01$) in the

Table 2. The Standard Deviation of the Arctic Mean 2 m Air Temperature (SAT, °C), Sea Ice Area (SIA, 10^{12} m^2), Latent Heat Flux (LH, W m^{-2}), Sensible Heat Flux (SH, W m^{-2}), Net Shortwave Radiation (SW, W m^{-2}), and Net Longwave Radiation (LW, W m^{-2}), for Winter and Summer, Respectively

Season	Climate	SAT	SIA	LH[a]	SH[a]	LW[a]	SW[a]
DJF	CTRL	0.57	0.23	0.59	0.66	0.51	0.01
	$2\times CO_2$	0.73	0.51	0.98	0.64	0.96	0.02
	$4\times CO_2$[b]	0.21	0.03	0.78	0.57	0.78	0.02
JJA	CTRL	0.09	0.23	0.22	0.16	0.33	1.48
	$2\times CO_2$	0.20	0.17	0.34	0.15	0.51	1.09
	$4\times CO_2$[b]	0.20	<0.01	0.37	0.15	0.61	1.33

[a]The radiation and heat fluxes are average values over the ocean and sea ice areas. All series are decadally smoothed prior to computing the standard deviation.
[b]In the $4\times CO_2$ climate some small localized areas near Greenland with high variability have a considerable influence on the average values of the radiative and turbulent fluxes.

CTRL and $4\times CO_2$ climate to −0.97 ($p < 0.01$) in the $2\times CO_2$ climate, showing that the relationship remains strong with climate warming. This temperature-sea-ice coupling operates mainly through enhanced variability of longwave radiation and latent heat fluxes over areas with most sea ice variability in CTRL and $2\times CO_2$ (not shown).

In the CTRL climate, the dominant SAT variability is located on the Atlantic side of the Arctic, near the sea ice margin (Figure 3a). At this location, the variability in sea ice concentration peaks as well. The local standard deviation of SAT reaches values of over 5°C over the Greenland Sea and the eastern Barents Sea (not shown). Over the central Arctic Ocean, however, CTRL sea ice is too thick for leads to form in relatively mild winters, explaining why the decadal temperature variability over the central Arctic in the current climate is
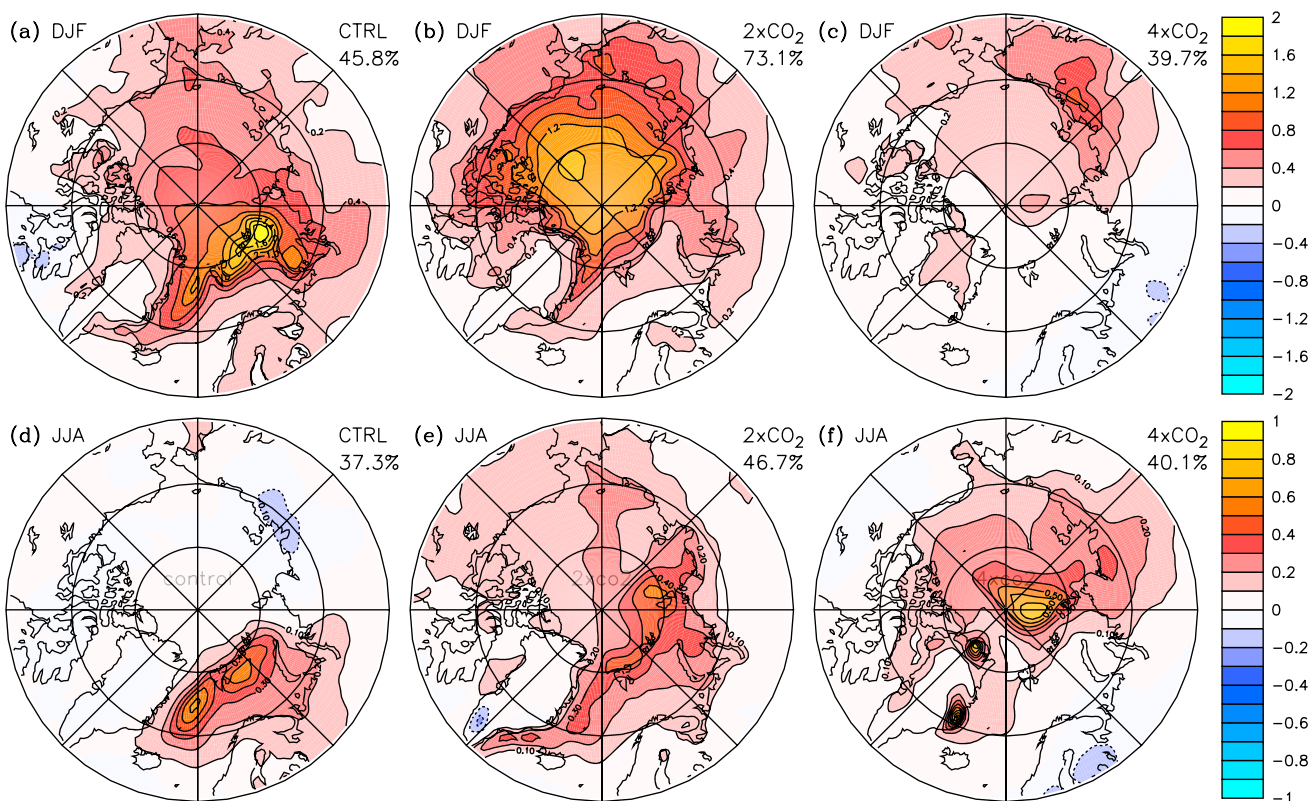

Figure 3. Leading EOF of Arctic (computed over 70–90°N) SAT, represented as the regression of SAT (K) on the normalized principal component time series (depicted in Figure 4) for (a, d) CTRL, (b, e) $2\times CO_2$, and (c, f) $4\times CO_2$, for winter and summer, respectively. The total variance explained by each pattern is indicated.
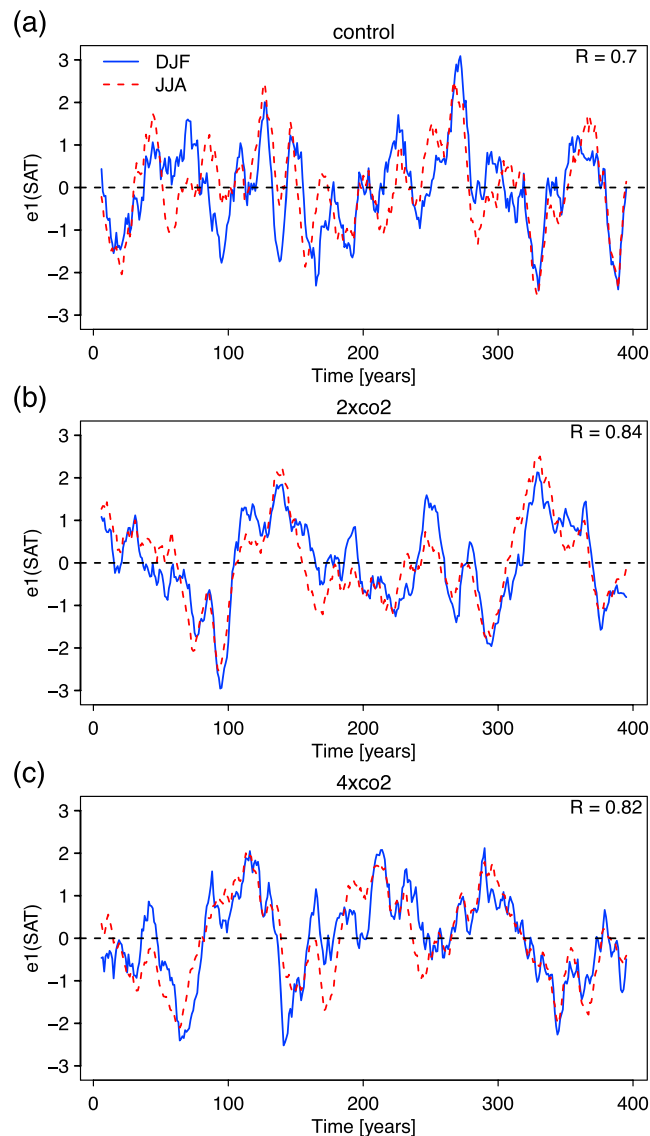
Figure 4. Time series of principal components of the first EOF of Arctic (70–90°N) SAT, normalized by its standard deviation for (a) CTRL, (b) 2×CO$_2$, and (c) 4×CO$_2$, for winter (blue) and summer (red dashed). The correlation coefficient between the two time series is indicated.

relatively small (less than 1°C). Note that the narrow region of relatively thin sea ice in the present-day climate is related to the geometry of the Arctic basin, which currently blocks the southward extension of (thin) sea ice [*Eisenman*, 2010].

In the 2×CO$_2$ climate, the temperature variability shifts northward along with the sea ice edge (Figure 3b) together with enhanced upward fluxes in latent heat and longwave radiation. However, the largest increase in variability is found farther north over the central Arctic Ocean where variability is up to 4 times as large as in CTRL. In this warm climate, the central Arctic Ocean also experiences the strongest variability in the latent heat and longwave radiation fluxes as well as in sea ice concentration (not shown), confirming again the strong link between variability in temperature and sea ice concentration. Due to thinner sea ice in this warm climate, the sea ice pack is more fragile and vulnerable over basically the entire Arctic Ocean, resulting in enhanced fluctuations of its total area, and therefore stronger decadal variability (Table 2). Related to this, *Van der Linden et al.* [2014] found that sea ice is most sensitive to temperature perturbations between 50 and 60% ice concentration, which equals the average sea ice concentration over the central Arctic basin in the

$2\times CO_2$ climate. In $4\times CO_2$, the absence of sea ice goes hand in hand with reduced temperature variability over the entire Arctic region (Figures 1c and 3c).

The variability of winter ice area and SAT is thus higher in moderately warmer climates compared to present-day values, which is related to a larger part of the sea ice cover that is vulnerable to melt. For stronger warming and further reductions in sea ice area, this effect vanishes and the variability drops off again. *Goosse et al.* [2009] find a similar dependency on the mean state for summer Arctic sea ice extent, which they explain by the shape of the Arctic basin that limits the sea ice area; currently, the most sensitive marginal ice zone in the present-day climate would occur in regions where the continents bordering the Arctic Ocean are situated. The larger variability in winter in the $2\times CO_2$ climate suggests that this mechanism is also effective in winter but that it will become relevant only at a later stage of warming. When the climate becomes so warm that even winter sea ice disappears, the temperature variability is further diminished by strong damping of the ocean.

3.2.2. Summer Variability

Summer variability is much weaker than in winter, except in the $4\times CO_2$ climate (Table 2). Summer variability of SAT becomes slightly larger in the warmer climates, whereas the variability of SIA drops off.

In the CTRL climate, the variance of summer SAT is much smaller than in winter, whereas the variance of SIA is the same in both seasons (Table 2). In this climate, sea ice survives during the summer (Table 1) meaning that summer SAT variability is bounded by the melting point temperature of sea ice and therefore smaller than in winter. The SIA variability itself is probably restricted by the presence of the surrounding continents. *Goosse et al.* [2009] found that the variance peaks for a mean September ice extent of around 3×10^6 km^2 (which is mainly due to geometrical restrictions), which in EC-Earth occurs somewhere between the CTRL and $2\times CO_2$ climate states (Table 1). The coupling between SIA and SAT variability is quite strong (Figure 2a; $r = -0.73$, $p < 0.01$) and is primarily associated with variability in net shortwave radiation through the ice-albedo feedback (Table 2), which is active mainly over the marginal ice zone in the Atlantic sector of the Arctic.

In the $2\times CO_2$ climate, SIA and SAT variability are still strongly coupled (Figure 2b; $r = -0.88$, $p < 0.01$), even though the mean SIA in summer shrinks to only 1×10^6 km^2 and virtually disappears in September (Table 1). The standard deviation of SIA obviously goes to 0 when sea ice almost disappears in the $4\times CO_2$ climate (Figure 2c). In the (nearly) sea-ice-free summers of the warm climates, the magnitude of SAT variability is approximately twice as large as in the CTRL climate. The atmosphere-ocean interaction is enhanced through increased variability in the latent heat flux and net longwave radiation, which averaged over the Arctic are almost twice as large in $4\times CO_2$ compared to the CTRL climate (Table 2). The variability of shortwave radiation reduces as sea ice disappears, which is clearly visible in the Arctic mean values of the $2\times CO_2$ climate (Table 2) but not in the $4\times CO_2$ climate due to some small localized peaks of very high variability near Greenland that affect the Arctic mean values.

In short, summer SIA variability in the CTRL climate is probably restricted by the surrounding continents, but in warmer climates the shrinking area becomes the limiting factor. Furthermore, melting sea ice restricts summer SAT variability, but in the absence of sea ice, summer SAT variability increases (partly) through enhanced surface fluxes. Locally, sea ice thus plays an important role for the decadal SAT variability. Sea ice cover itself is sensitive to meridional heat transfer variations into the Arctic through the large-scale circulation, which we will investigate in the next section.

4. Changes in the Atmospheric Circulation

To improve our understanding of the feedback mechanisms and interactions of the Arctic ice-ocean-atmosphere coupled system involved in (changes in) ADV, we examine here how the atmospheric circulation changes with climate warming. We concentrate on atmospheric pressure patterns, which influence the large-scale atmospheric circulation, and thereby the atmospheric heat transports toward the Arctic region. Changes in the atmospheric circulation can have a large effect on oceanic transports to and from the Arctic Ocean through changes in wind patterns and associated ocean currents. Furthermore, the redistribution and transport of sea ice through changed atmospheric circulation patterns have been found to affect sea ice melt or growth [*Kwok and Rothrock*, 1999; *Rigor et al.*, 2002; *Zhang et al.*, 2000]. Air-sea interaction is not a one-way process, however. Local temperature anomalies and related changes in sea ice can alter the atmospheric circulation through thermal forcing from below [*Slonosky et al.*, 1997; *Alexander et al.*, 2004; *Dethloff et al.*, 2006; *Budikova*, 2009]. In the following, we will briefly analyze the basic characteristics of the mean
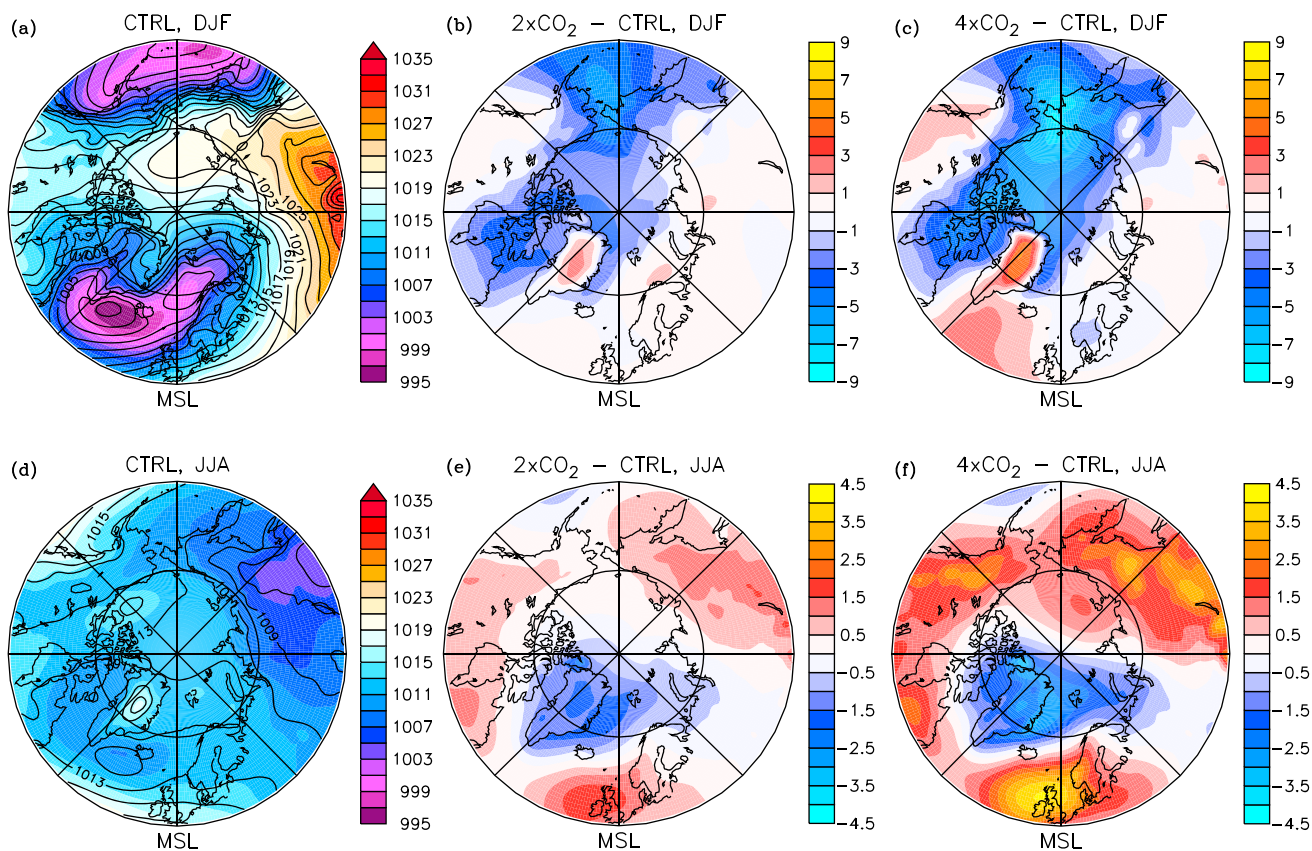
Figure 5. Mean sea level pressure (hPa) at 50–90°N in the (a, c) CTRL climate, and differences with respect to the CTRL climate in (b, e) 2×CO_2 and (c, f) 4×CO_2, for winter (Figures 5a–5c) and summer (Figures 5d–5f). The contour lines in the CTRL climate represent the average SLP of the ERA-20C reanalysis averaged over the period 1990–2010.

climatological distribution of SLP and how this changes as the climate warms. Thereafter, we will examine the spatial structure of the leading modes of SLP variability and how this alters with climate warming.

4.1. Mean State of SLP

Figure 5 depicts the mean SLP pattern in the CTRL climate, as well as its changes relative to the CTRL for 2×CO_2 and 4×CO_2, for both winter and summer. The spatial patterns in the CTRL climate are virtually the same as those derived from the ERA-20C reanalysis data (shown in contours). In winter, when the circulation is strongest, three well-known "centers of action" dominate the pressure field: the Siberian High over east central Asia, the Icelandic Low off the southeast coast of Greenland, and the Aleutian Low in the North Pacific Ocean. Compared to the mean winter SLP field in CTRL, the strengthening of the Aleutian Low in the warmer climates is quite remarkable. In warming climates, this low extends northeastward over the Bering Sea region, following the retreating sea ice margin and hence the region of large surface temperature gradients. These horizontal temperature gradients are associated with strong cyclone development processes and might contribute to the northward shift of the Pacific storm track. Furthermore, the jet stream influences the speed and direction of travel of the extratropical cyclones and thereby the location and strength of the storm track [*Shaw et al.*, 2016]. The changes in the mean pressure field might therefore well be related to the intensification of the westerly jet in a warming world [*Mizuta*, 2012]. The model results are supported by the observed increase in the number and strength of cyclones entering the Arctic during the second half of the twentieth century [*Graham and Diaz*, 2001; *Zhang et al.*, 2004].

In summer, the three centers of action are much weaker: the Aleutian Low has disappeared, the Icelandic Low is quite weak and extends over eastern Canada, and the Siberian High is replaced by a broad area of low pressure. In warmer climates, the Icelandic Low deepens and extends northward over the Greenland Sea, while the northern flank of the Azores High strengthens as well. The northward extension of the Icelandic Low might be related to the strong temperature gradients over the sea ice edge, which migrate northward in warmer
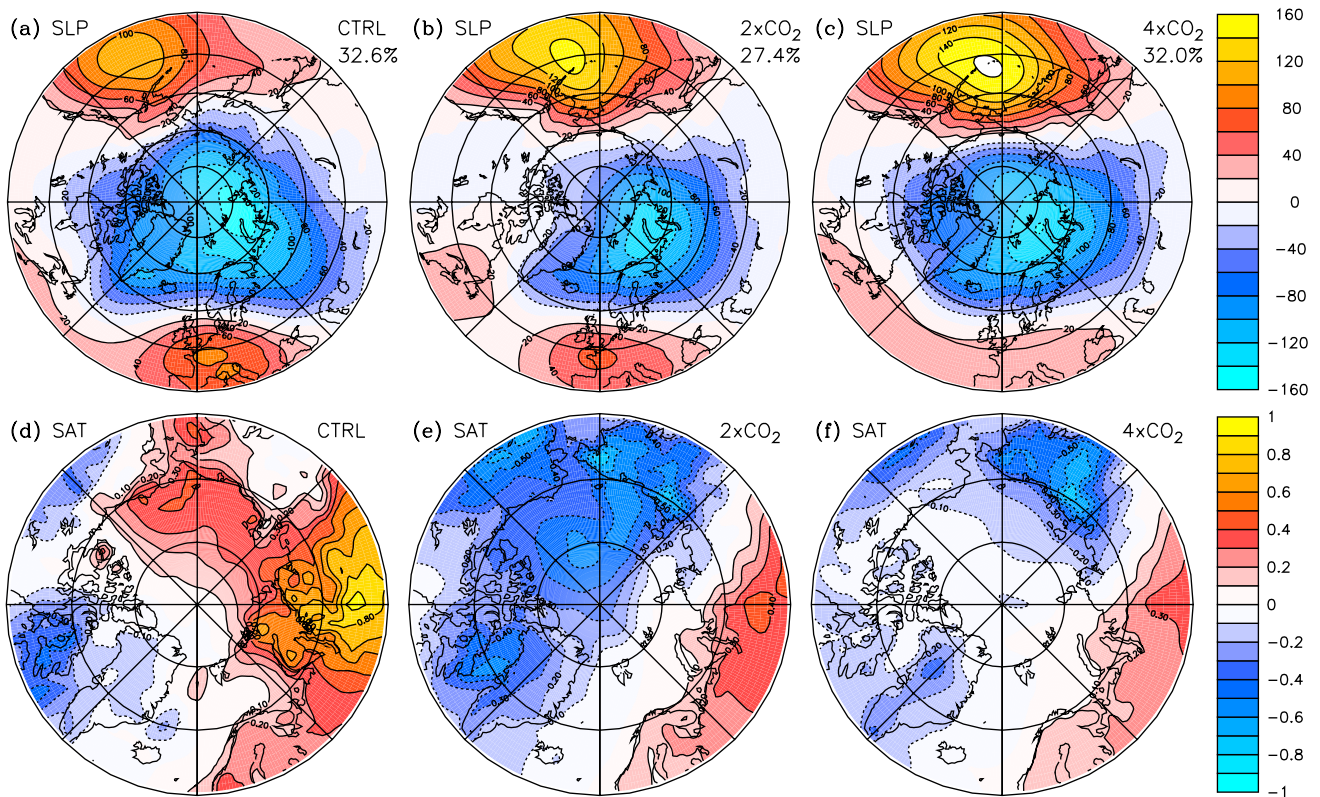
Figure 6. First EOF of Northern Hemisphere (computed over 20–90°N) winter (DJF) sea level pressure anomalies (Pa) for filtered time series, represented as the regression of SLP on the normalized principal component time series e1(SLP) for the (a) CTRL, (b) 2×CO$_2$, and (c) 4×CO$_2$ experiments. The total variance explained by each pattern is indicated. Regression of winter 2 m temperature (K) on e1(SLP) for the (d) CTRL, (e) 2×CO$_2$, and (f) 4×CO$_2$ experiments.

climates, and the related cyclogenesis [*Inoue et al.*, 2012]. Furthermore, the very strong temperature gradient between the Greenland Ice Sheet (which in the model is essentially represented as a white mountain) and adjacent milder ocean might enhance baroclinic conditions in this region as well. The high-pressure anomaly over the British Isles is likely part of an atmospheric response to the decelerating Atlantic meridional overturning circulation in global climate models as discussed by *Haarsma et al.* [2015]. This anomaly pattern induces increased westerlies through an enhanced north-south pressure gradient.

In a warming climate, we thus find that the Aleutian Low intensifies in winter and that the Icelandic Low becomes stronger in summer. Both centers of low pressure also migrate northward, which is consistent with the warming-related poleward migration of the jet stream in climate model simulations in the respective seasons [*Barnes and Polvani*, 2013], although the full effect of Arctic warming on the jet stream might well be more complicated [*Barnes and Screen*, 2015].

4.2. Variability of SLP and Associated Temperature Changes

Climate warming-related changes in the mean state of the large-scale atmospheric circulation are more extensively studied than changes in its variability. To gain insight into the signature of changes in SLP variability, and how this relates to temperature and sea ice variations, we use EOF analysis. As a first step, we compare the leading EOF modes of SLP variability and related patterns of SAT anomalies between the various climate states. The spatial patterns associated with the three dominant SLP modes are, respectively, labeled E1(SLP), E2(SLP), and E3(SLP). The associated principal component time series are labeled e1(SLP), e2(SLP), and e3(SLP), respectively. For each mode, we only discuss the winter patterns, since these are stronger and more distinct than their summer equivalents.

E1(SLP), which explains 27.4–32.6% of the variance, is characterized by a prominent pressure anomaly over the central Arctic basin, and two pressure anomalies of opposite sign over the North Pacific and North Atlantic basins (Figure 6a–6c). This mode is generally known as the Arctic Oscillation (AO) [*Thompson and Wallace*, 1998] or Northern Annular Mode (NAM), which is the hemispheric expression of the more regional NAO.
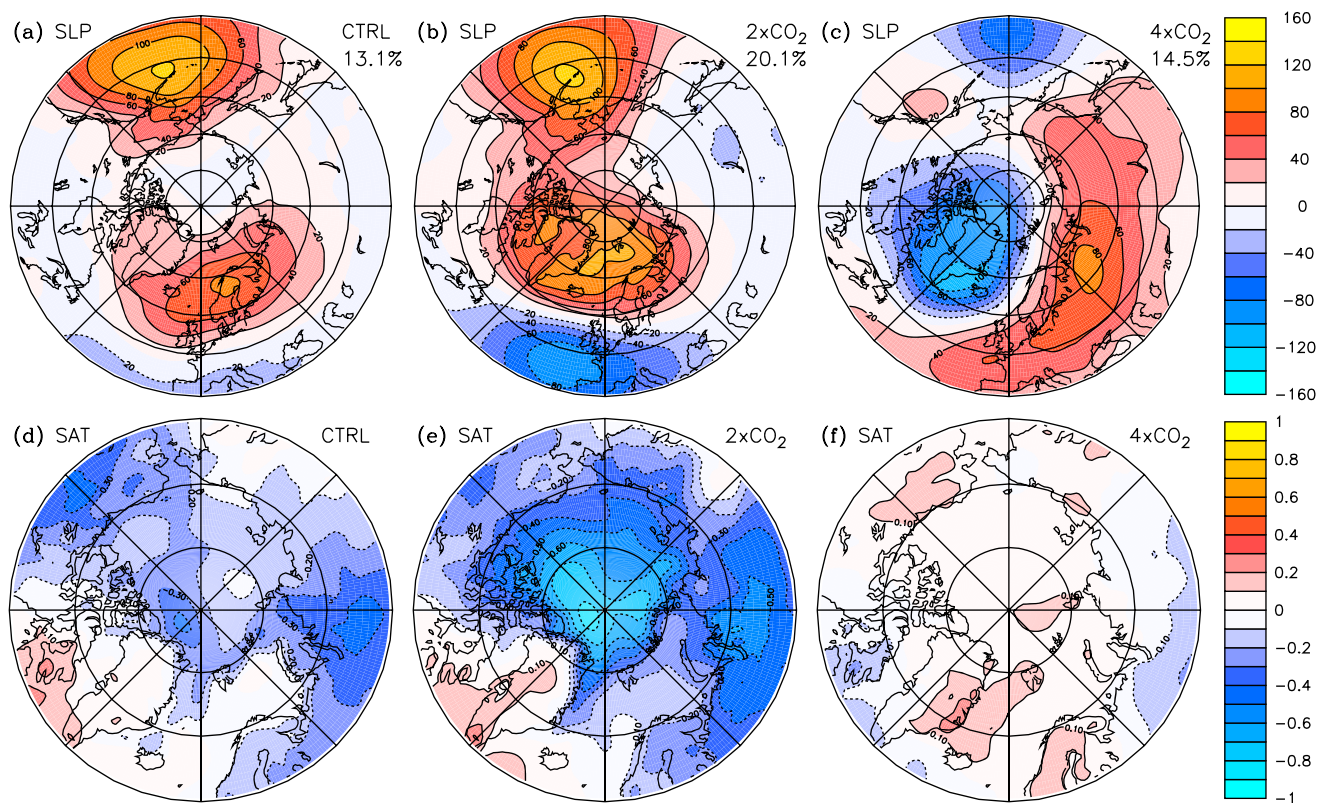
Figure 7. Second EOF of Northern Hemisphere (computed over 20–90°N) winter (DJF) sea level pressure anomalies (Pa) for filtered time series, represented as the regression of SLP on the normalized principal component time series e2(SLP) for the (a) CTRL, (b) $2\times CO_2$, and (c) $4\times CO_2$ experiments. The total variance explained by each pattern is indicated. Regression of winter 2 m temperature (K) on e2(SLP) for the (d) CTRL, (e) $2\times CO_2$, and (f) $4\times CO_2$ experiments.

This simulated E1(SLP) resembles the leading mode derived from observations [e.g., *Holland*, 2003], although the simulated amplitude is obviously smaller owing to the decadal smoothing. The principal component time series of this mode, e1(SLP), is a measure of the strength of the AO as a function of time: the AO index. In winter, e1(SLP) splits the Arctic into two regions, based on the related pattern of temperature variability (Figures 6d–6f).

Even though e1(SAT) is not significantly linked to e1(SLP) in the CTRL climate ($r = 0.22$, $p = 0.13$) owing mainly to the dipole-like nature of the SAT regression pattern, e1(SLP) affects the regional pattern of SAT anomalies in the present-day climate, agreeing with results of *Graversen* [2006]. During positive phases of the AO/NAM (low pressure over the central Arctic) the European/Siberian continent is relatively mild and the Canadian continent cold (Figure 6d). Related to these SAT patterns, sea ice reduces over most of the Arctic Ocean (not shown).

In warmer climates during winter, positive temperature anomalies associated with a positive AO index reach less far into the Arctic region and remain mostly over the western Eurasian continent (Figures 6e and 6f). The negative temperature anomalies on the Canadian side of the Arctic occupy a much larger region, including east Siberia and the Pacific sector of the central Arctic Ocean. As a result, a positive AO index relates to cold Arctic anomalies and extended sea ice in warmer climates as shown by the relatively strong correlation between e1(SAT) and e1(SLP) ($r = 0.51$, $p < 0.01$), whereas it coincides with warm Arctic anomalies and reduced sea ice in the present-day climate. Remarkably, our model simulations thus indicate that the SAT signature associated with a positive mode of the AO changes with climate warming.

The AO-related shift in the temperature pattern is likely associated with the strengths and locations of the centers of action. The influence of the Pacific center becomes stronger and shifts northwestward in milder climates, while the influence of the Atlantic center weakens substantially (Figures 6a–6c), consistent with *Choi et al.* [2010]. On the Atlantic side of the Arctic the north-south pressure gradient decreases with climate warming, leading to weaker zonal winds and less advection of relatively warm air and ocean water from the
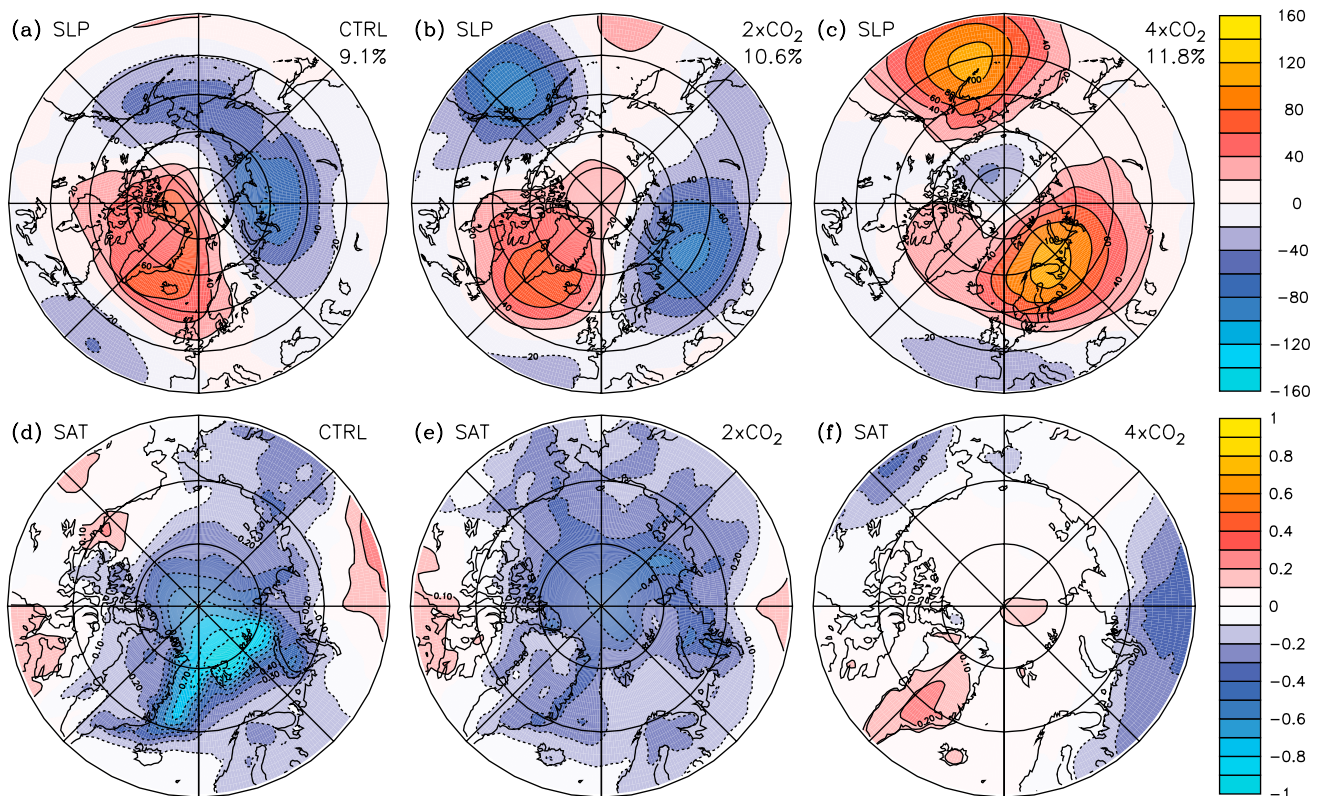
Figure 8. Third EOF of Northern Hemisphere (computed over 20–90°N) winter (DJF) sea level pressure anomalies (Pa) for filtered time series, represented as the regression of SLP on the normalized principal component time series e3(SLP) for the (a) CTRL, (b) 2×CO$_2$, and (c) 4×CO$_2$ experiments. The total variance explained by each pattern is indicated. Regression of winter 2 m temperature (K) on e3(SLP) for the (d) CTRL, (e) 2×CO$_2$, and (f) 4×CO$_2$ experiments.

North Atlantic region to the Eurasian continent. Conversely, on the Pacific side, the north-south pressure gradient increases with climate warming, leading to stronger zonal winds and more eastward advection of relatively cold Siberian air over the Arctic Ocean. In warmer climates, enhanced advection of comparatively cold Siberian continental air over the Arctic Ocean and reduced advection of warm North Atlantic air over Eurasia might contribute to the cold anomalies in the central Arctic region that are associated with a positive AO index.

E2(SLP), which explains 13.1–20.1% of the decadal variability, also relates to temperature and sea ice over the Arctic region (Figure 7). In winter, this second mode is mainly associated with the strength of the Aleutian Low in CTRL and 2×CO$_2$, which links to the Pacific Decadal Oscillation (PDO) [*Mantua et al.*, 1997]. A stronger Aleutian Low (positive PDO) has been associated with transport of warm, moist air over Alaska into the Arctic [*Hartmann and Wendler*, 2005]. The regression of SAT on e2(SLP) shows that in winter, weaker Aleutian and Icelandic Lows are associated with lower temperature anomalies and sea ice growth over most of the Arctic, and higher temperatures over the east Canadian Arctic (Figure 7). In the CTRL climate the SAT regression coefficients on e2(SLP) are largest over the central Arctic, compared to the dipolar SAT signal related to e1(SLP), which also explains the relatively strong correlation between e1(SAT) and e2(SLP) ($r = 0.58$, $p < 0.01$). The temperature changes related to e2(SLP) are especially large in the 2×CO$_2$ climate, in which fluctuations in sea ice concentration amplify the total climate variability in the central Arctic Ocean.

Finally, E3(SLP) in the CTRL and 2×CO$_2$ climate is characterized by a dipole of opposite surface pressures across the Arctic (Figures 8a and 8b). This mode is often referred to as the Arctic Dipole Anomaly (DA) [*Wu et al.*, 2006] and is associated with a strong meridional component in the surface wind anomaly and related sea ice motion [*Watanabe et al.*, 2006]. Although this mode is not distinct on the hemispheric scale (20–90°N) according to North's rule of thumb [*North et al.*, 1982], it appears as a distinct EOF mode of SLP over only the Arctic region (70–90°N) and is therefore included in our analysis. A high-pressure anomaly over Greenland and low-pressure anomaly over Siberia are linked to lower SAT in the Arctic region (Figures 8d and 8e). Using the National Centers for Environmental Prediction-National Center for Atmospheric Research reanalysis,

this "negative" phase of the DA is associated with a strengthened Beaufort gyre and with reduced sea ice over the Barents and the Greenland Seas [*Wu et al.*, 2006]. EC-Earth exhibits similar DA-related sea ice characteristics in the CTRL climate (not shown). In regions where sea ice diverges, open water and/or thin sea ice appears and the heat flux from the ocean can directly influence the local air temperature. Arctic SAT changes related to the DA are especially large over regions with high sea ice variability (not shown). Surface winds associated with the DA seem to be of crucial importance for sea ice motion and thereby significantly affect the surface air temperature distribution.

For $4\times CO_2$, the third mode of SLP variability resembles the second mode of CTRL and $2\times CO_2$, and likewise, the second mode resembles the third mode (DA), but the associated temperature changes are fairly small and both modes are not distinct.

The leading modes of SLP variability change with climate warming, even though the EOFs are partially constrained by the geography of the Arctic region (continental boundaries and orography). Furthermore, the differences in the corresponding SAT anomalies between the various climate states are partly determined by the locations of high variability in sea ice.

5. Variability of the Coupled Fields of SLP and SAT

In the previous section, we have found that the variability of SLP and the associated SAT patterns change toward warmer climates. In sections 5.1 and 5.2, we reverse this analysis by examining what changes in SLP anomalies are related to the dominant changes in SAT variability. We use the first principal component of SAT north of 70°N (e1(SAT); Figure 4) for spatial regressions of SLP, thereby implicitly including regions outside the Arctic where SAT varies in phase with temperatures in the Arctic (Figure 3).

Changes in the variability of the atmospheric circulation could be associated with oceanic and atmospheric heat transport anomalies. Therefore, we also assess to what extent the total oceanic (OHT) and atmospheric (AHT) heat transport toward the Arctic are involved in ADV. Here OHT is evaluated as the residual of net surface fluxes and ocean heat storage, while AHT is calculated from the net surface and top-of-the-atmosphere fluxes. Note that in the computation of the OHT and AHT diagnostics it is assumed that the EC-Earth model conserves perfectly the energy internally and does not take into account any unforced trends as discussed by *Hobbs et al.* [2016]. We will discuss winter and summer variability separately.

To further assess and confirm the relationships between Northern Hemisphere SLP and Arctic SAT, we also examine the coupled modes of variability of SAT north of 70°N and the SLP field north of 20°N in section 5.3. For this purpose, we use the method of singular value decomposition (SVD) on the cross-covariance matrix between SAT and SLP. In this way, we will identify the coupled spatial patterns that explain most of the covariance between the two variables.

5.1. Winter Patterns
Figures 9a–9c show wintertime regressions of the SLP anomalies on e1(SAT). The atmospheric SLP pattern associated with e1(SAT) changes gradually from the CTRL climate toward warmer climate states.

In the present-day climate, high Arctic temperature anomalies are associated with a strong low-pressure area centered over the Greenland Sea that extends well into the Arctic basin and high-pressure anomalies over the Gulf of Alaska and east Siberia. These spatial structures extend upward into the troposphere, where the associated patterns in geopotential height at 850, 500, and 200 hPa exhibit similar characteristics (not shown), indicating an equivalent-barotropic structure with little variation in the wind patterns with height. The intense low-pressure anomaly over the Greenland Sea, which is clearly associated with poleward advection of warm air in the present climate, becomes less important for SAT variability toward warmer climate states (Figures 9a–9c). In contrast, the importance of the low-pressure anomaly over the Aleutian Islands and the high-pressure anomaly over Siberia increases with climate warming.

In the CTRL climate, the atmospheric pressure signature that is related to decadal variability (Figure 9a) is quite firmly connected to E3(SLP) (Figure 8a), being the DA pattern. The related SAT pattern (Figure 8d) exhibits a rather large SAT signal over the regions where the largest SAT variability occurs (Figure 3a). The prominent role of the DA pattern in terms of Arctic SAT variability in the current climate is further emphasized by the relatively
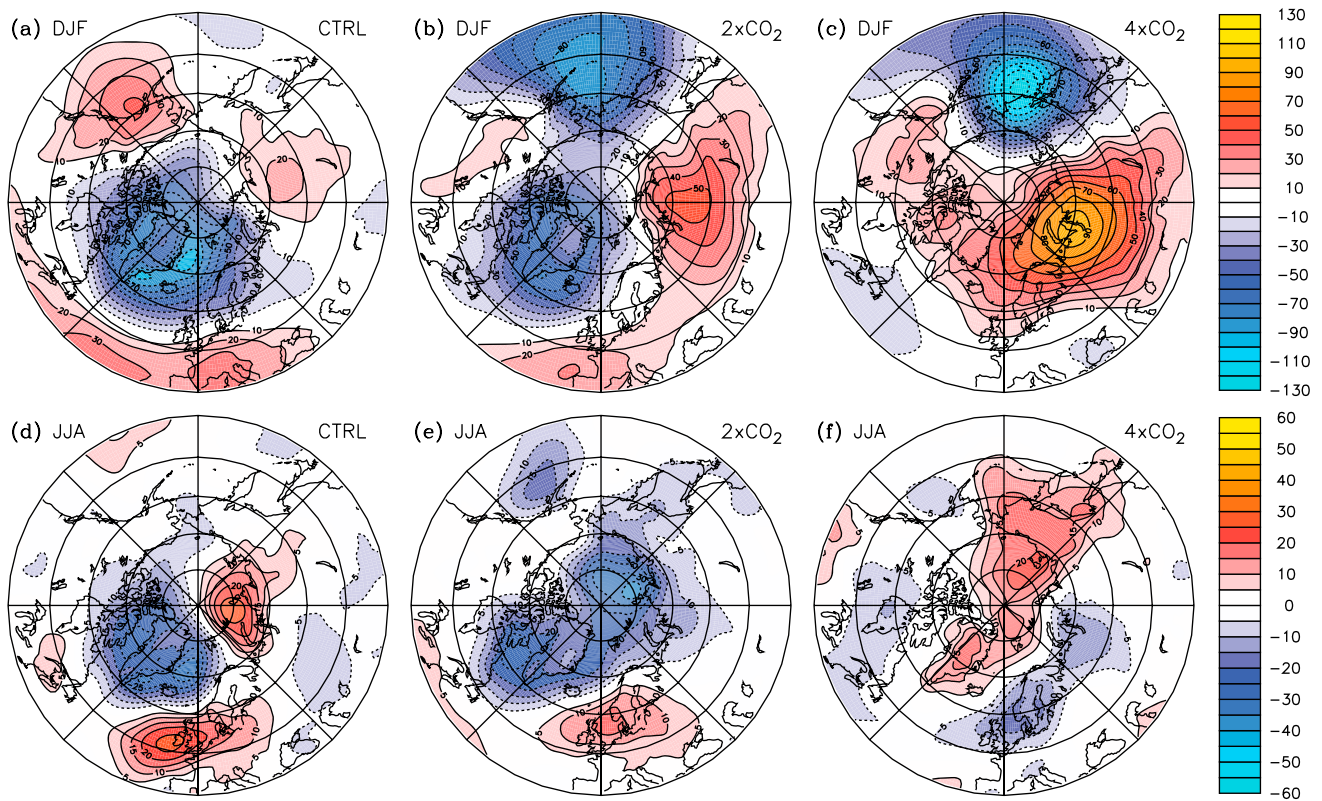
Figure 9. Regression of SLP anomalies (Pa) on the normalized principal component time series e1(SAT) (depicted in Figure 4) for (a, d) CTRL, (b, e) 2×CO$_2$, and (c, f) 4×CO$_2$, for winter (Figures 9a–9c) and summer (Figures 9d–9f), respectively.

strong pattern correlation between E1(SAT) and the regression of SAT on e3(SLP) ($r = 0.82$), whereas E1(SAT) has a much weaker correlation to the SAT regression patterns on e1(SLP) ($r = 0.54$) and on e2(SLP) ($r = 0.58$).

We also find a relatively strong relation between ocean heat transport and Arctic SAT variability during winter, which is strongest when SAT leads by 3 years ($r = -0.51$, $p < 0.01$), suggesting that in winter months the ocean responds to Arctic temperature changes. During warm periods, OHT anomalies reduce the climatological mean OHT at 70°N, which in winter is directed northward.

In the 2×CO$_2$ climate, anomalous Arctic warming is characterized by a deep low-pressure area over the Aleutian Islands and a high-pressure anomaly over Siberia (Figure 9b). This pattern has characteristics of both the second and the third EOF of SLP (Figures 7b and 8b). Moreover, the SAT signatures associated with E2(SLP) and E3(SLP) (Figures 7e and 8e) both depict the strongest SAT signal over the central Arctic. This coincides with the region of dominant SAT variability in this warm climate (Figure 3b), meaning that E2(SLP) and E3(SLP) contribute significantly to Arctic SAT variability. The strong links between the second and third EOF of SLP and SAT variability are confirmed by the strong pattern correlation between E1(SAT) and the regression of SAT on e2(SLP) ($r = 0.82$) and on e3(SLP) ($r = 0.78$).

Also, in the 2×CO$_2$ climate, an anomalous outflow of ocean heat is strongly related to Arctic warming ($r = 0.66$, $p < 0.01$). This correlation is even (slightly) stronger when SAT leads by 1 year, implying that winter OHT responds to the corresponding SAT changes. In both the CTRL and 2×CO$_2$ climate, reduced northward OHT during winter is thus mainly associated with a warmer Arctic in the previous winter.

In the warmest climate state, the relation with the Siberian High and Aleutian Low on SAT variability becomes even stronger than in 2×CO$_2$, whereas the relation with the Icelandic Low vanishes (Figure 9c). This pattern exhibits similarities with the AO-like E1(SLP) pattern (Figure 6c), which is confirmed by the rather firm pattern correlation between E1(SAT) and the regressed field of SAT on e1(SLP) ($r = 0.83$), while the pattern

correlations with the SAT regression maps on the other principal component time series are rather weak ($r = 0.49$ for e2(SLP) and $r = 0.23$ for e3(SLP)).

To summarize, winter SLP patterns associated with SAT variability change considerably as the climate warms. Different SLP modes are firmly linked to SAT variability during the various stages of warming: the DA-like E3(SLP) pattern for CTRL, E2(SLP) and E3(SLP) for $2\times CO_2$, and the AO-like E1(SLP) for $4\times CO_2$, suggesting that the dominant circulation mode associated with wintertime Arctic decadal variability is likely to change with future warming. When the climate warms, the wintertime Aleutian Low considerably deepens in the climatological mean state and also plays a more prominent role in winter SAT variability.

5.2. Summer Patterns

In summer, SLP patterns related to SAT variability are more regional and more diverse among the three climate states compared to winter. In the CTRL climate, the warm phase of decadal variability is associated with a regional atmospheric pattern characterized by a low-pressure anomaly over Greenland, which forms a tripole of surface pressure with high-pressure anomalies over the eastern Arctic basin and off the coast of Ireland (Figure 9d). This pattern bears some resemblance to the NAO, a dipole between middle and high latitudes but then with northward shifted high- and low-pressure centers, as well as to the DA, a dipole of opposite pressure anomalies across the Arctic Ocean. The pressure pattern indicates a southwesterly flow near the Barents Sea entrance.

We found an indication that the summer OHT is leading ADV in the current climate. The summer circulation pattern is accompanied by an anomalous northward inflow of ocean heat transport, which is confirmed by a strong relation between total OHT at 70°N and Arctic SAT ($r = 0.79$, $p < 0.01$). As a result, in summer more heat is trapped in the Arctic region, which reinforces Arctic summer warming. A strong correlation between winter Arctic SAT and summer OHT ($r = 0.74$, $p < 0.01$) suggests that the additional summer heat is carried over to the winter as well. Hence, during anomalously warm periods the summer heat transport by the ocean reinforces Arctic warming throughout the year, indicating that ocean heat transport amplifies Arctic temperature variability. The delayed and reduced northward OHT anomalies in winter could be a consequence of the reduced meridional temperature gradient in the ocean due to the warming.

In the summer of the $2\times CO_2$ climate, the influence of the high-pressure center over the eastern Arctic on the SAT variability vanishes (Figure 9e). Instead, warm Arctic summers relate to the anomalous low-pressure system over Greenland, which in this climate state merges with a newly formed low-pressure anomaly over the central Arctic. In summer, there is also a strong link between northward OHT and Arctic SAT ($r = 0.93$, $p < 0.01$) in this mild climate. Similar to the CTRL climate, winter surface air temperatures are also strongly linked with summer OHT ($r = 0.88$, $p < 0.01$). The enhanced summer OHT anomalies into the Arctic during warm periods are thus also present in the $2\times CO_2$ climate and amplify Arctic warming throughout the year.

Finally, in the $4\times CO_2$ climate, the summer SLP distribution associated with warm Arctic summers is completely different compared to the two other climate states (Figure 9f). In this climate, a high-pressure anomaly centered over the Arctic Ocean with extensions over Greenland and east Siberia and a low-pressure anomaly over the North Sea are related to Arctic warm phases. In contrast to the other two climates, the relation between total northward OHT and Arctic temperatures is negligible ($r = -0.09$, $p = 0.57$). The correlation between northward atmospheric heat transport and Arctic warming in summer is quite strong and negative ($r = -0.61$, $p < 0.01$), implying that the net northward AHT at 70°N in summer is reduced during warm phases and reduces Arctic temperature variability.

These results indicate that ADV is associated with seasonally dependent changes in the atmospheric circulation and oceanic and atmospheric heat transports toward the Arctic region. However, finer details of these changes in the large-scale circulation in the ocean and the atmosphere should be the topic of subsequent research.

5.3. SVD Analysis

By inspecting the coupled spatial patterns of the SVD modes and their similarities to the independent EOF modes and related regression fields of SAT and SLP, we test the robustness of our previous findings. Here we focus on the wintertime patterns, to be able to make the comparison with the independent EOF modes of SLP. The spatial patterns of SLP associated with the two dominant SVD modes are respectively labeled S1(SLP)
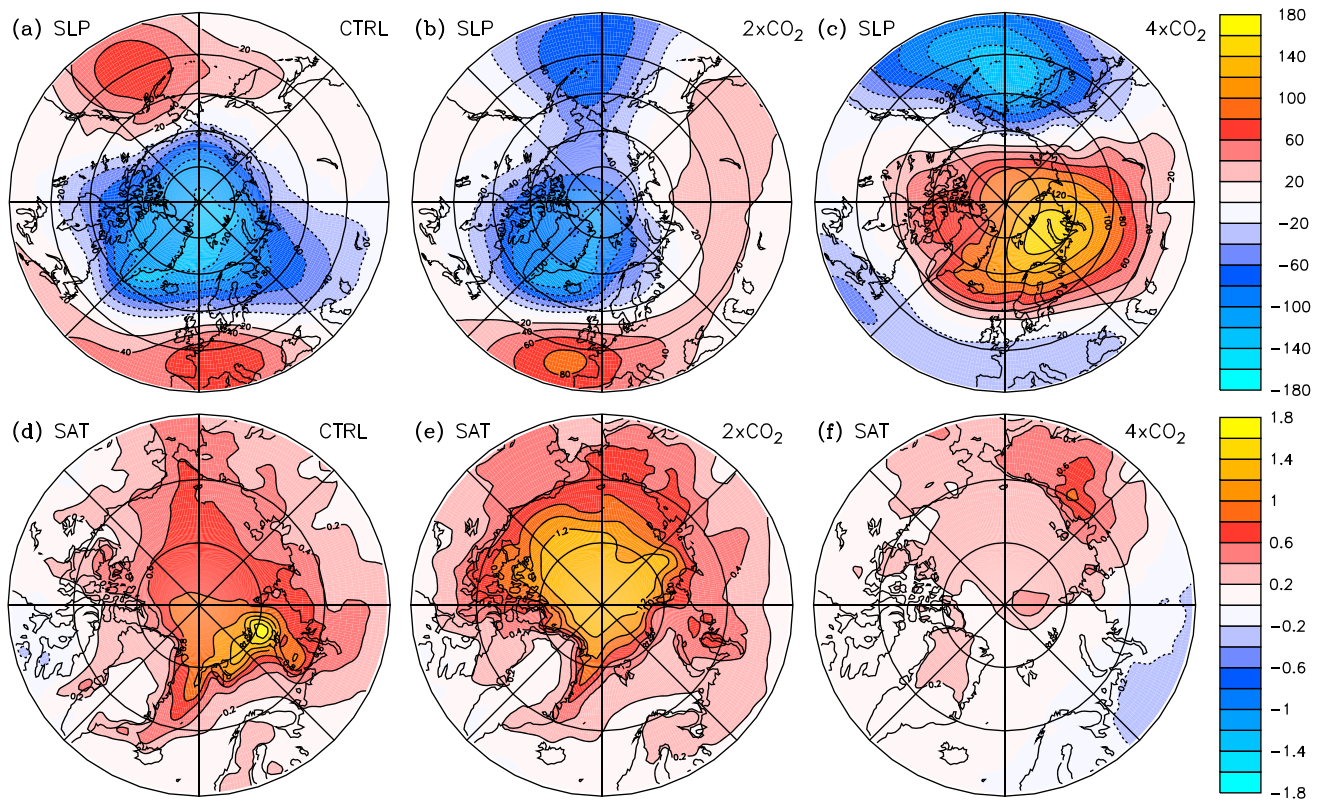
Figure 10. Spatial patterns of the first SVD coupled mode of wintertime (DJF) Northern Hemisphere (20–90°N) SLP and Arctic (70–90°N) SAT for the (a, d) CTRL, (b, e) $2\times CO_2$, and (c, f) $4\times CO_2$ climate, respectively. Spatial patterns are represented as homogenous regression maps (i.e., regression maps of SLP anomalies (Pa) on normalized s1(SLP) time series and of SAT anomalies (K) on normalized s1(SAT) time series).

and S2(SLP). In a similar way, the spatial patterns of SAT associated with the two dominant SVD modes are labeled S1(SAT) and S2(SAT).

Figures 10 and 11 show the spatial patterns of the two leading SVD modes for the CTRL, $2\times CO_2$, and $4\times CO_2$ climate. The SVD patterns are presented as homogenous regression maps, which indicate the spatial pattern and the typical amplitude of the variables represented by the SVD modes. Table 3 displays the squared covariance fractions (SCF) explained by the first two SVD modes and the correlation coefficients (r) between the expansion coefficients of SLP and SAT. These coupling correlations between the SAT and SLP time series indicate the strength of the coupling. Our discussion focuses only on the first two SVD modes since they explain most of the squared covariance between the two fields. Also, these two modes are the only distinct modes following North's rule of thumb [*North et al.*, 1982].

The first SVD mode of the coupled SAT and SLP fields accounts for 57–82% of the total square covariance in the three climate states (Table 3). The winter atmospheric SLP (Figures 10a–10c) and SAT (Figures 10d–10f) patterns associated with S1 differ between the CTRL climate and the warmer climate states.

In the present-day climate, SLP oscillations centered over the Arctic basin and Greenland Sea are coupled with SAT fluctuations over the entire Arctic with strongest oscillations over the Barents Sea region. The S1(SLP) pattern has characteristics of both E1(SLP) (Figure 6a) and E3(SLP) (Figure 8a), suggesting that the AO and DA pattern explain most of the wintertime covariance between Northern Hemisphere SLP and Arctic SAT in the CTRL climate. Furthermore, the S1(SAT) pattern strongly resembles E1(SAT) (Figure 3a), indicating that this SVD mode explains most of the circulation-related SAT variability in the Arctic in the CTRL climate.

In the $2\times CO_2$ climate, S1(SLP) closely resembles E2(SLP) (Figure 7b), showing that the atmospheric mode that dominates the coupled variability changes with climate warming. For SAT, the first coupled mode S1(SAT) connects strongly to E1(SAT) (Figure 3b), suggesting that S1 captures the dominant SAT variability in the Arctic region. E2(SLP) thus provides information on the dominant decadal variability of SAT in the Arctic, indicating that the role of the Aleutian Low in SAT variability strengthens in this mild climate state.
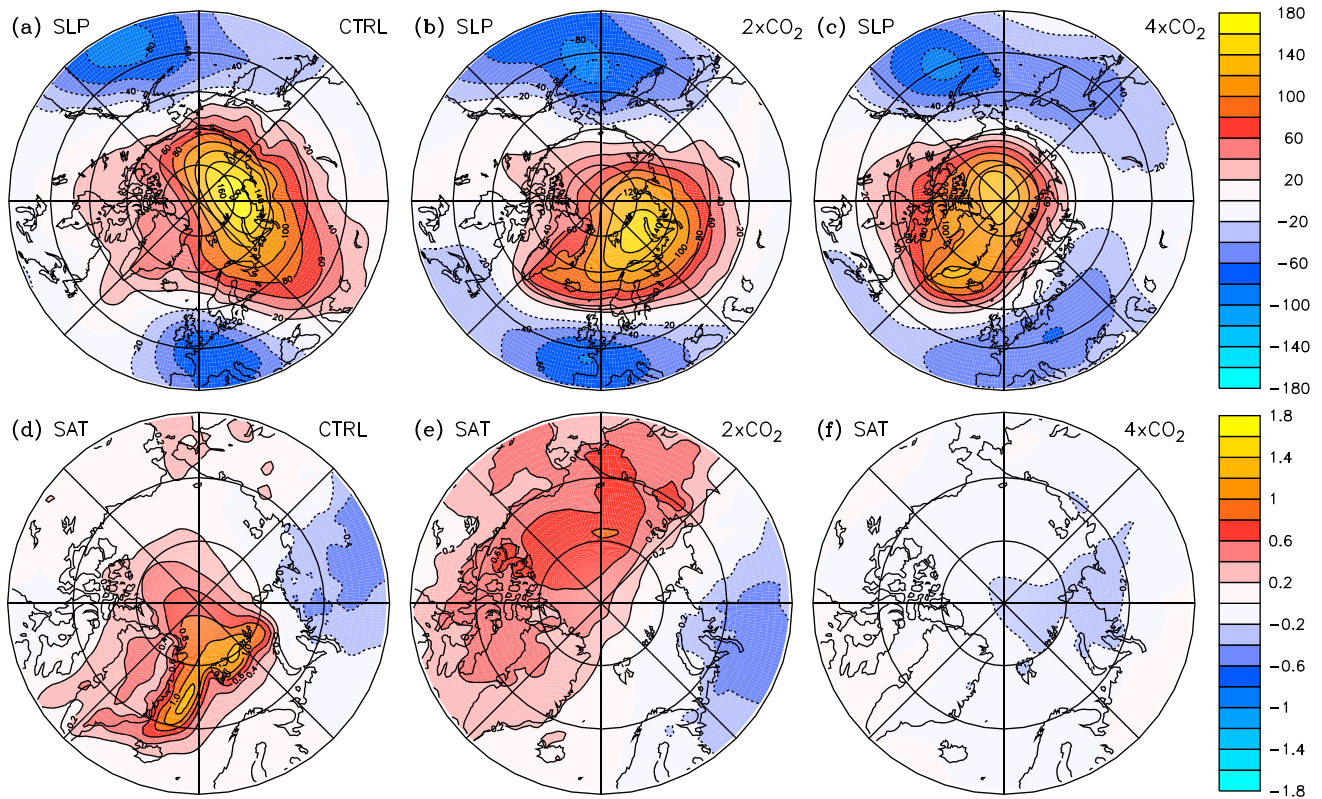
Figure 11. Spatial patterns of the second SVD coupled mode of wintertime (DJF) Northern Hemisphere (20–90°N) SLP and Arctic (70–90°N) SAT for the (a, d) CTRL, (b, e) $2\times CO_2$, and (c, f) $4\times CO_2$ climate, respectively. Spatial patterns are represented as homogenous regression maps (i.e., regression maps of SLP anomalies (Pa) on normalized s2(SLP) time series and of SAT anomalies (K) on normalized s2(SAT) time series).

The S2 mode (Figure 11) accounts for 13–21% of the total square covariance (Table 3). In the CTRL and $2\times CO_2$ climate, the centers of action of S2(SLP) are located over the Barents-Kara Sea, over the Aleutian Islands, and south of the United Kingdom (Figures 11a and 11b). The S2(SLP) mode closely resembles the Arctic Oscillation pattern (Figures 6a and 6b). The related S2(SAT) patterns (Figures 11d and 11e) show a dipolar SAT signal over the Arctic region, somewhat similar to the SAT regression maps associated with the AO (Figures 6d and 6e). In the CTRL climate, a positive SLP anomaly over the Kara Sea is associated with positive temperature anomalies over the Greenland Sea (Figures 11a and 11d). In the $2\times CO_2$ climate, the positive temperature anomalies associated with a positive SLP anomaly over the Kara Sea extend over the entire Canadian and Alaskan side of the Arctic (Figures 11b and 11e).

In the $4\times CO_2$ climate, both S1(SLP) and S2(SLP) (Figures 10c and 11c) have characteristics of the S2(SLP) mode of the CTRL and $2\times CO_2$ climate (Figures 11a and 11b) that were discussed above, indicating an important role for the AO in this warm climate.

The SVD analyses thus confirm the main conclusions that were found with the EOF analyses and regression maps in the previous sections.

Table 3. Square Covariance Fraction (SCF) and Coupling Correlation Coefficient Between the Expansion Coefficients of SAT and SLP (r) Corresponding to the Two Leading SVD Modes for the Winter Season (DJF)[a]

	CTRL		$2\times CO_2$		$4\times CO_2$	
Mode	SCF	r	SCF	r	SCF	r
1	67%	0.62 [0.21]	82%	0.73 [0.22]	57%	0.59 [0.22]
2	21%	0.68 [0.20]	13%	0.77 [0.21]	20%	0.57 [0.21]

[a]In brackets are the 95% significance levels for the correlations.

6. Summary and Conclusions

In this study, we investigate how Arctic decadal variability in SAT changes as the climate warms. For this purpose three 550 year long simulations with the state-of-the-art climate model EC-Earth using present-day, double, and quadrupled CO_2 forcing have been carried out. The final 400 years of these simulations have been evaluated, meaning that the climate states studied here are in (quasi-)equilibrium. Our approach concentrates on the large-scale atmospheric circulation patterns in the Northern Hemisphere, how these contribute to ADV in the present climate, and how (much) these change in warmer climate states. To obtain a comprehensive picture of ADV, we chose not to focus on a specific atmospheric mode or a particular region. In contrast to previous studies, we assess three dominant atmospheric modes north of 20°N and include the entire Arctic and surrounding areas in our analysis. Finally, seasonal variability is taken into account by considering winter and summer conditions separately.

Decadal variability (and changes therein) should be taken into account when analyzing climate trends in the Arctic region. The difficulty in separating forced trends from (unforced) decadal variability in observations is related to the data having either too scattered temporal coverage or too low temporal resolution (e.g., in proxy data) to accurately capture decadal variability. Model simulations are therefore an appropriate and indispensable tool to study this type of variability, notwithstanding the caveats associated with climate models, especially when using only one model (e.g., model-dependent physics).

It is found that the relationship between sea ice and temperature variability changes nonlinearly when the climate warms. SAT and SIA variability are strongest in 2×CO_2 in winter, when the average sea ice concentration north of 70°N is about 55%. A broken sea ice cover with intermittent leads at a coverage around 50% is indeed most vulnerable to temperature changes, as shown by *Van der Linden et al.* [2014]. Moreover, *Goosse et al.* [2009] found an increased variability of Arctic summer ice extent when the climate warms, which confirms our finding. This suggests that in the near future, Arctic variability will very likely become stronger. When Arctic warming continues and sea ice melts away almost completely in the winter, SAT variability over the Arctic region will strongly diminish, since all ice-related feedbacks will disappear as well. These include a more intense turbulent heat release to the atmosphere in winter when sea ice is reduced. The increase in variability in 2×CO_2 is especially relevant because the atmospheric CO_2 concentration is currently rising. Since climate warming and retreating sea ice are associated with stronger ADV, it is vitally important to consider ADV changes when assessing trends in Arctic warming from model simulations/projections.

In warmer climates the mean large-scale atmospheric circulation changes, with intensified Aleutian (winter) and Icelandic Lows (summer). Moreover, the variability of the atmospheric circulation changes as well and also its impact on surface air temperature anomalies. Several earlier studies have assessed the link between the AO/NAO and Arctic warming or sea ice decline [e.g., *Holland*, 2003; *Goosse and Holland*, 2005], finding mostly a positive but relatively weak relation. In our model, a positive AO index is indeed associated with less sea ice in the current climate. This is consistent with observations in the late 1980s through early 1990s, when a decline in summer ice concentration in the eastern Arctic Ocean and the Barents and Nordic Seas was associated with a positive trend in the AO. However, this relationship does not hold for more recent observations. Since the mid-1990s, the AO is in a near-neutral or negative state, yet sea ice decline is ongoing and likely even accelerating—a feature termed the Arctic Climate Paradox by *Overland and Wang* [2005]. Our results suggest that this paradox might be (at least partly) attributed to changes in the AO and the associated SAT pattern. In our simulations of warmer-than-present climates, there is still a difference in temperature signal between the Eurasian and Canadian sectors of the Arctic region, but the transition region between positive and negative temperature anomalies associated with the AO shifts toward Siberia. This suggests that the ADV contribution of the various atmospheric modes is dependent on the mean climate state.

We find that different atmospheric modes dominate circulation-related ADV during subsequent stages of climate warming. Hence, links between atmospheric circulation modes and Arctic climate variability are not necessarily constant as the climate warms, meaning that transitions between circulation types determining Arctic variability might be expected when the climate system continues to warm.

All results presented here are based on one particular climate model. The obvious disadvantage of this approach is that the results may depend (partially) on model physics/parameterizations. Similar analyses using other climate models are therefore necessary to infer if our conclusions are robust. Nonetheless, this study provides valuable new insights into how Arctic decadal variability might change with climate warming.

References

Alexander, M. A., U. S. Bhatt, J. E. Walsh, M. S. Timlin, J. S. Miller, and J. D. Scott (2004), The atmospheric response to realistic Arctic sea ice anomalies in an AGCM during winter, *J. Clim.*, *17*(5), 890–905.

Barnes, E. A., and L. Polvani (2013), Response of the midlatitude jets, and of their variability, to increased greenhouse gases in the CMIP5 models, *J. Clim.*, *26*(18), 7117–7135, doi:10.1175/JCLI-D-12-00536.1.

Barnes, E. A., and J. A. Screen (2015), The impact of Arctic warming on the midlatitude jet-stream: Can it? Has it? Will it?, *Wiley Interdiscip. Rev. Clim. Change*, *6*(3), 277–286, doi:10.1002/wcc.337.

Bouillon, S., M. A. Morales Maqueda, V. Legat, and T. Fichefet (2009), An elastic-viscous-plastic sea ice model formulated on Arakawa B and C grids, *Ocean Modell.*, *27*(3–4), 174–184, doi:10.1016/j.ocemod.2009.01.004.

Budikova, D. (2009), Role of Arctic sea ice in global atmospheric circulation: A review, *Global Planet. Change*, *68*(3), 149–163, doi:10.1016/j.gloplacha.2009.04.001.

Choi, D. H., J. S. Kug, W. T. Kwon, F. F. Jin, H. J. Baek, and S. K. Min (2010), Arctic Oscillation responses to greenhouse warming and role of synoptic eddy feedback, *J. Geophys. Res.*, *115*, D17103, doi:10.1029/2010JD014160.

Cohen, J., et al. (2014), Recent Arctic amplification and extreme mid-latitude weather, *Nat. Geosci.*, *7*, 627–637, doi:10.1038/ngeo2234.

Comiso, J. C., and D. K. Hall (2014), Climate trends in the Arctic as observed from space, *Wiley Interdiscip. Rev. Clim. Change*, *5*(3), 389–409, doi:10.1002/wcc.277.

Day, J. J., J. C. Hargreaves, J. D. Annan, and A. Abe-Ouchi (2012), Sources of multi-decadal variability in Arctic sea ice extent, *Environ. Res. Lett.*, *7*(3), 034011, doi:10.1088/1748-9326/7/3/034011.

Dethloff, K., et al. (2006), A dynamical link between the Arctic and the global climate system, *Geophys. Res. Lett.*, *33*, L03703, doi:10.1029/2005GL025245.

Eisenman, I. (2010), Geographic muting of changes in the Arctic sea ice cover, *Geophys. Res. Lett.*, *37*, L16501, doi:10.1029/2010GL043741.

Fichefet, T., and M. A. Morales Maqueda (1997), Sensitivity of a global sea ice model to the treatment of ice thermodynamics and dynamics, *J. Geophys. Res.*, *102*, 12,609–12,646, doi:10.1029/97JC00480.

Goosse, H., and M. M. Holland (2005), Mechanisms of decadal Arctic climate variability in the Community Climate System Model, Version 2 (CCSM2), *J. Clim.*, *18*(17), 3552–3570, doi:10.1175/JCLI3476.1.

Goosse, H., O. Arzel, C. M. Bitz, A. de Montety, and M. Vancoppenolle (2009), Increased variability of the Arctic summer ice extent in a warmer climate, *Geophys. Res. Lett.*, *36*, L23702, doi:10.1029/2009GL040546.

Graham, N. E., and H. F. Diaz (2001), Evidence for intensification of North Pacific winter cyclones since 1948, *Bull. Am. Meteorol. Soc.*, *82*, 1869–1893, doi:10.1175/1520-0477(2001)082<1869:EFIONP>2.3.CO;2.

Graversen, R. G. (2006), Do changes in the midlatitude circulation have any impact on the Arctic surface air temperature trend?, *J. Clim.*, *19*(20), 5422–5438, doi:10.1175/JCLI3906.1.

Haarsma, R. J., F. M. Selten, and S. S. Drijfhout (2015), Decelerating Atlantic meridional overturning circulation main cause of future west European summer atmospheric circulation changes, *Environ. Res. Lett.*, *10*(9), 094007, doi:10.1088/1748-9326/10/9/094007.

Hartmann, B., and G. Wendler (2005), The significance of the 1976 Pacific climate shift in the climatology of Alaska, *J. Clim.*, *18*(22), 4824–4839, doi:10.1175/JCLI3532.1.

Hazeleger, W., et al. (2012), EC-Earth V2.2: Description and validation of a new seamless Earth system prediction model, *Clim. Dyn.*, *39*(11), 2611–2629, doi:10.1007/s00382-011-1228-5.

Hezel, P. J., T. Fichefet, and F. Massonnet (2014), Modeled Arctic sea ice evolution through 2300 in CMIP5 extended RCPs, *Cryosphere*, *8*(4), 1195–1204, doi:10.5194/tc-8-1195-2014.

Hobbs, W., M. D. Palmer, and D. Monselesan (2016), An energy conservation analysis of ocean drift in the CMIP5 global coupled models, *J. Clim.*, *29*(5), 1639–1653, doi:10.1175/JCLI-D-15-0477.1.

Holland, M. M. (2003), The North Atlantic Oscillation-Arctic oscillation in the CCSM2 and its influence on Arctic climate variability, *J. Clim.*, *16*(16), 2767–2781, doi:10.1175/1520-0442(2003)016<2767:TNAOOI>2.0.CO;2.

Inoue, J., M. E. Hori, and K. Takaya (2012), The role of Barents sea ice in the wintertime cyclone track and emergence of a warm-Arctic cold-Siberian anomaly, *J. Clim.*, *25*(7), 2561–2569, doi:10.1175/JCLI-D-11-00449.1.

Kay, J. E., M. M. Holland, and A. Jahn (2011), Inter-annual to multi-decadal Arctic sea ice extent trends in a warming world, *Geophys. Res. Lett.*, *38*, L15708, doi:10.1029/2011GL048008.

Koenigk, T., and L. Brodeau (2014), Ocean heat transport into the Arctic in the twentieth and twenty-first century in EC-Earth, *Clim. Dyn.*, *42*(11–12), 3101–3120, doi:10.1007/s00382-013-1821-x.

Koenigk, T., L. Brodeau, R. G. Graversen, J. Karlsson, G. Svensson, M. Tjernström, U. Willén, and K. Wyser (2013), Arctic climate change in 21st century CMIP5 simulations with EC-Earth, *Clim. Dyn.*, *40*(11–12), 2719–2743, doi:10.1007/s00382-012-1505-y.

Kwok, R., and D. A. Rothrock (1999), Variability of Fram Strait ice flux and North Atlantic Oscillation, *J. Geophys. Res.*, *104*(1998), 5177–5189.

Li, C., J. S. von Storch, and J. Marotzke (2013), Deep-ocean heat uptake and equilibrium climate response, *Clim. Dyn.*, *40*(5–6), 1071–1086, doi:10.1007/s00382-012-1350-z.

Madec, G. (2008), NEMO ocean engine, *Tech. Rep.*, Institut Pierre-Simon Laplace, IPSL, France.

Mantua, N. J., S. R. Hare, Y. Zhang, J. M. Wallace, and R. C. Francis (1997), A Pacific interdecadal climate oscillation with impacts on salmon production, *Bull. Am. Meteorol. Soc.*, *78*(6), 1069–1079, doi:10.1175/1520-0477(1997)078<1069:APICOW>2.0.CO;2.

Mizuta, R. (2012), Intensification of extratropical cyclones associated with the polar jet change in the CMIP5 global warming projections, *Geophys. Res. Lett.*, *39*, L19707, doi:10.1029/2012GL053032.

North, G. R., T. L. Bell, and R. F. Cahalan (1982), Sampling errors in the estimation of empirical orthogonal functions, *Mon. Weather Rev.*, *110*(7), 699–706, doi:10.1175/1520-0493(1982)110<0699:SEITEO>2.0.CO;2.

Overland, J. E., and M. Wang (2005), The Arctic climate paradox: The recent decrease of the Arctic Oscillation, *Geophys. Res. Lett.*, *32*, L06701, doi:10.1029/2004GL021752.

Poli, P., et al. (2016), ERA-20C: An atmospheric reanalysis of the twentieth century, *J. Clim.*, *29*(11), 4083–4097, doi:10.1175/JCLI-D-15-0556.1.

Polyakov, I. V., G. V. Alekseev, R. V. Bekryaev, U. S. Bhatt, R. Colony, M. A. Johnson, V. P. Karklin, D. Walsh, and A. V. Yulin (2003), Long-term ice variability in Arctic marginal seas, *J. Clim.*, *16*(12), 2078–2085, doi:10.1175/1520-0442(2003)016<2078:LIVIAM>2.0.CO;2.

Poulsen, C. J., and J. Zhou (2013), Sensitivity of arctic climate variability to mean state: Insights from the Cretaceous, *J. Clim.*, *26*(18), 7003–7022, doi:10.1175/JCLI-D-12-00825.1.

Rigor, I. G., J. M. Wallace, and R. L. Colony (2002), Response of sea ice to the Arctic Oscillation, *J. Clim.*, *15*(18), 2648–2663, doi:10.1175/1520-0442(2002)015<2648:ROSITT>2.0.CO;2.

Shaw, T. A., et al. (2016), Storm track processes and the opposing influences of climate change, *Nat. Geosci.*, *9*(9), 656–664, doi:10.1038/ngeo2783.

Slonosky, V. C., L. A. Mysak, and J. Derome (1997), Linking Arctic sea-ice and atmospheric circulation anomalies on interannual and decadal timescales, *Atmos. Ocean*, *35*(3), 333–366, doi:10.1080/07055900.1997.9649596.

Swart, N. C., J. C. Fyfe, E. Hawkins, J. E. Kay, and A. Jahn (2015), Influence of internal variability on Arctic sea-ice trends, *Nat. Clim. Change*, *5*(2), 86–89, doi:10.1038/nclimate2483.

Taylor, K. E., R. J. Stouffer, and G. A. Meehl (2012), An overview of CMIP5 and the experiment design, *Bull. Am. Meteorol. Soc.*, *93*(4), 485–498, doi:10.1175/BAMS-D-11-00094.1.

Thompson, D. W. J., and J. M. Wallace (1998), The Arctic Oscillation signature in the wintertime geopotential height and temperature fields, *Geophys. Res. Lett.*, *25*(9), 1297–1300, doi:10.1029/98GL00950.

Valcke, S., A. Caubel, D. Declat, and L. Terray (2003), OASIS3 ocean atmosphere sea ice soil user's guide, *Prism Project Rep.*, *2*.

Van der Linden, E. C., R. Bintanja, W. Hazeleger, and C. A. Katsman (2014), The role of the mean state of Arctic sea ice on near-surface temperature trends, *J. Clim.*, *27*(8), 2819–2841, doi:10.1175/JCLI-D-12-00617.1.

Van der Linden, E. C., R. Bintanja, W. Hazeleger, and R. G. Graversen (2016), Low-frequency variability of surface air temperature over the Barents Sea: Causes and mechanisms, *Clim. Dyn.*, *47*(3–4), 1247–1262, doi:10.1007/s00382-015-2899-0.

Watanabe, E., J. Wang, A. Sumi, and H. Hasumi (2006), Arctic dipole anomaly and its contribution to sea ice export from the Arctic Ocean in the 20th century, *Geophys. Res. Lett.*, *33*, L23703, doi:10.1029/2006GL028112.

Wu, B., J. Wang, and J. E. Walsh (2006), Dipole anomaly in the winter Arctic atmosphere and its association with sea ice motion, *J. Clim.*, *19*(2), 210–225.

Zhang, J., D. Rothrock, and M. Steele (2000), Recent changes in Arctic sea ice: The interplay between ice dynamics and thermodynamics, *J. Clim.*, *13*(17), 3099–3114, doi:10.1175/1520-0442(2000)013<3099:RCIASI>2.0.CO;2.

Zhang, L., and C. Wang (2013), Multidecadal North Atlantic sea surface temperature and Atlantic meridional overturning circulation variability in CMIP5 historical simulations, *J. Geophys. Res. Oceans*, *118*, 5772–5791, doi:10.1002/jgrc.20390.

Zhang, X., J. E. Walsh, J. Zhang, U. S. Bhatt, and M. Ikeda (2004), Climatology and interannual variability of Arctic cyclone activity: 1948–2002, *J. Clim.*, *17*(12), 2300–2317, doi:10.1175/1520-0442(2004)017<2300:CAIVOA>2.0.CO;2.